Homogeneous Redox Mediators Applied to Li–S Batteries

RESEARCH ARTICLE OPEN ACCESS

Homogeneous Redox Mediators Applied to Li–S Batteries

N. Tan Luong[1] | Sergi Sànchez-Ribot[1] | Roza Bouchal[1] | Patrik Johansson[1,2,3]

[1]Department of Physics, Chalmers University of Technology, Gothenburg, Sweden | [2]Department of Chemistry – Ångström, Uppsala University, Uppsala, Sweden | [3]ALISTORE—European Research Institute, CNRS FR 3104, Hub de l'Energie, Amiens, France

Correspondence: N. Tan Luong (tan.luong@chalmers.se; nntlu@dtu.dk) | Roza Bouchal (roza.bouchal@mpikg.mpg.de)

Received: 9 March 2026 | **Revised:** 13 April 2026 | **Accepted:** 16 April 2026

Keywords: cyclic voltammetry | electrochemical impedance spectroscopy | electrolytes | galvanostatic cycling | Li–S battery | metallocenes | polysulfide catholytes | quinones | Raman spectroscopy | redox mediators

ABSTRACT

Lithium–sulfur (Li–S) batteries are promising as next-generation energy storage, primarily due to their high theoretical specific energy density combined with a low-cost cathode active material. However, incomplete sulfur utilization, polysulfide (PS) shuttling, sluggish redox kinetics, etc. still limit their practical performance. Employing homogeneous redox mediators (RMs) to the electrolyte is one strategy to improve charge transfer and facilitate key solid–liquid transitions. While both metallocene and quinone-based RMs have shown promise, their reactivities with sulfur, PSs, and electrolyte components in general remain poorly understood. Here, we systematically investigate two metallocene RMs, decamethylferrocene (DmFc) and decamethylmanganocene (DmMn), and two quinone RMs, anthraquinone (AQ) and 1,4-bis(methylamino)-9,10-anthraquinone (NHQ), across various Li–S battery designs including sulfur-, PS catholyte-, and Li_2S-based active materials, and weakly solvating electrolytes. We show that the efficacy of these RMs is highly sensitive to sulfur speciation and electrolyte composition and that AQ is most versatile with suitable redox potential, high chemical stability, and efficient regeneration. Together, these findings provide guidelines for selecting RMs for specific Li–S battery technologies.

1 | Introduction

Lithium–sulfur (Li–S) batteries are promising candidates for energy storage as they offer high theoretical specific energy density at low materials cost [1]. However, the performance of traditional Li–S battery designs, based on a C/S composite cathode, is limited by two major intrinsic drawbacks. First, the electronically insulating nature of sulfur, and also of Li_2S, slows down charge transfer and causes sluggish redox kinetics, limiting the sulfur utilization. Second, the formation of highly soluble intermediate polysulfides (PSs, e.g., S_n^{2-} with $n = 2$–8) which diffuse between the electrodes (PS shuttling) continuously consumes active material [2, 3]. Combined, this results in low practical capacity and energy density, poor cyclability, and rapid capacity fading, hindering the commercialization of Li–S batteries.

Several approaches to mitigate these issues have been tried: new cathode designs (to improve electronic conductivity and better contain S) [4], electrolyte additives (to protect the lithium anode vs. PSs by, e.g., $LiNO_3$) [5], and new electrolyte designs (to limit/regulate the PS solubility by solvents [6–9], anions [10], and salt concentrations [10–12], etc.). A quite different approach is to deliberately dissolve PSs in the electrolyte to create a *catholyte* [13]. Initial trials by Rauh et al. [14] encountered rapid capacity losses, but the catholyte concept was later [15] revitalized and applied in redox–flow cells [16] and liquid cells [17], as well as traditional Li–S battery cells [4, 13, 18–21]. The catholyte approach renders a more uniform distribution of PSs, which improves deposition/dissolution kinetics and cycling stability, and supports high sulfur loadings. Nonetheless, the catholyte concept still faces significant challenges, such as limited specific capacity (~600–700 mAh/g), poor rate capability, and declining sulfur utilization upon extended cycling. Another alternative is

to use Li_2S as the cathode active material, sometimes paired with lithium-free anodes [22], but its low both electrical and ionic conductivity result in substantial activation overpotentials [23], and the initial de-lithiation involves sluggish solid–solid transitions in the absence of PSs [24].

Both sulfur utilization and charge transfer kinetics can be improved by applying redox mediators (RMs) [25, 26], an approach which is inspired by their established roles in biological redox cycles [27], dye sensitized solar cells [28], and Li–O_2 batteries [29]. In Li–S batteries RMs, either heterogeneous, immobilized on the electrode or separator, or homogeneous, soluble in the electrolyte, can indeed facilitate key solid–liquid, liquid–liquid, and liquid–solid transitions [2] involving both elemental sulfur, PSs, and Li_2S. Heterogeneous RMs, such as metals [30, 31], metal oxides [25, 32, 33]/sulfides [34, 35]/nitrides [36, 37], and polymeric carbon nitrides [38], all work by enhancing the PS adsorption at the cathode surface, thereby promoting charge transfer and improving the reversibility of the sulfur/Li_2S conversion. Their catalytic activity, however, often declines at high depth of discharge due to deposition of Li_2S passivation layers [39] that hinders the electron transfer. In contrast, homogeneous RMs undergo redox reactions at the electrode surfaces before diffusing into the electrolyte, where they react with sulfur or PSs, enabling more uniform charge transport. Prominent examples of homogeneous RMs are metallocenes [40] and quinones [41], which offer redox potentials tunable to match those of different PS transformations/reactions. The redox state of the RM influences different reactions: the reduced forms assist sulfur and/or long-chain PS reduction during discharge (Figure 1a), while the oxidized forms promote Li_2S and/or short-chain PS oxidation during charge (Figure 1b).

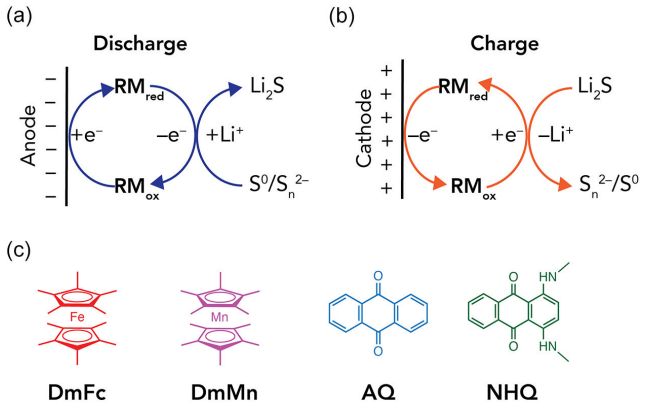

FIGURE 1 | Schematic of how RMs assist the conversions between sulfur and PSs during discharge (a) and charge (b). (c) Chemical structures of decamethylferrocene (DmFc), decamethylmanganocene (DmMn), anthraquinone (AQ), and 1,4-bis(methylamino) 9,10-anthraquinone (NHQ).

The roles of metallocene- and quinone-based RMs across different Li–S battery designs remain insufficiently understood, particularly with respect to how their activity depends on sulfur/PS speciation and electrolyte composition. We here investigate two metallocene-based RMs, decamethyl ferrocene (DmFc) and decamethyl manganocene (DmMn), and two quinone-based RMs, anthraquinone (AQ) and 1,4-bis(methylamino)-9,10-anthraquinone (NHQ) (Figure 1c), using electrochemical and spectroscopy techniques. Their activities and stabilities are evaluated in differently designed Li–S battery cells using (i) sulfur, (ii) PS catholytes, and (iii) Li_2S as the active materials, as well as using (iv) weakly solvating electrolytes (WSEs). Particular attention is given to the redox state of each RM during discharge and charge,

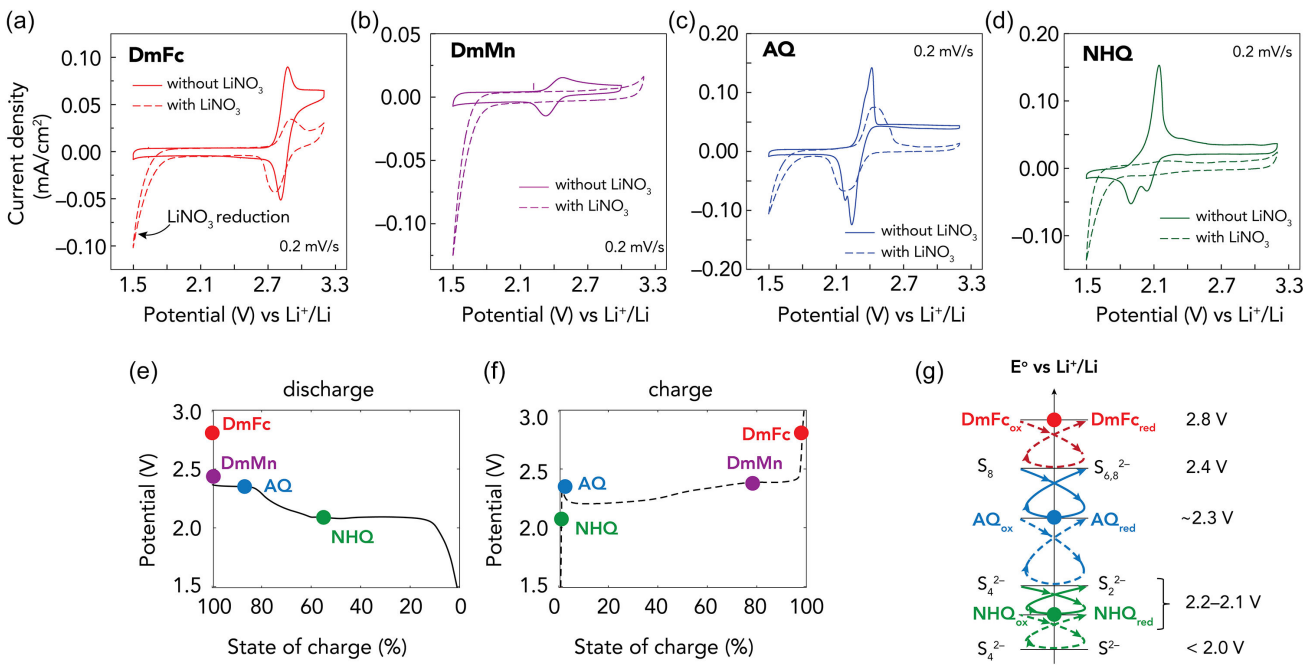

FIGURE 2 | Voltammograms of 1.0 M LiTFSI in DME:DOL electrolytes containing ~ 20 mM of (a) DmFc, (b) DmMn, (c) AQ, and (d) NHQ, with and without 0.3 M $LiNO_3$. Schematic representation of the redox potentials of RMs in comparison with the Li-S cell: (e) discharge and (f) charge profiles. (g) Schematic (not scaled) of the RMs' reactivity toward PSs using literature values [2, 42] and the gamma rule during discharge (solid lines) and charge (dash lines).

in order to identify which sulfur-based species they preferentially interact with and how this governs Li–S battery performance and stability. Furthermore, by correlating the RM chemistry with the sulfur speciation and electrolyte composition, we provide new mechanistic insights able to guide rational selection of RMs for practical Li–S batteries.

2 | Results and Discussion

We start with an analytical study of the different RMs and electrolytes before Li–S battery cell performance is presented. A standard electrolyte, composed of 1.0 M lithium bis(trifluoromethanesulfonyl)imide (LiTFSI) and 0.3 M $LiNO_3$ in a 1:1 (v/v) mixture of 1,2-dimethoxyethane (DME) and 1,3-dioxolane (DOL), was used unless specified otherwise. First, the basic electrochemistry of electrolytes with different RMs included is presented in order to monitor stability and redox potentials and thus potential usefulness for Li–S batteries. Second, we probe this by their influence on the performance of Li–S battery cells using (i) a traditional C/S composite cathode, (ii) catholytes, and (iii) a Li_2S cathode. Finally, based on the knowledge gained, we investigate if/how WSEs, created by replacing DME with 1,2-bis(1,1,2,2-tetrafluoroethoxy)ethane (TFEE), alter the RM operation.

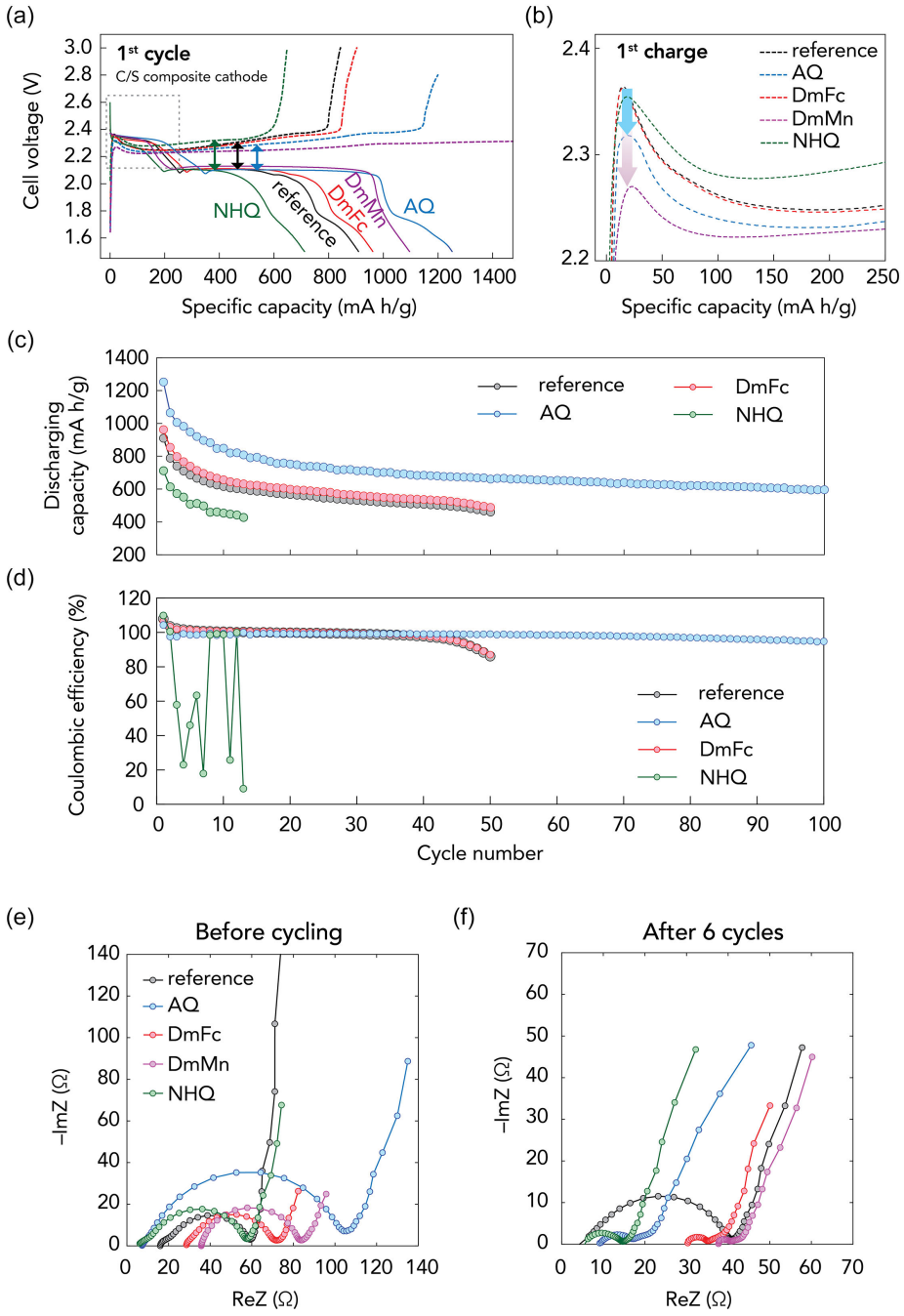

FIGURE 3 | (a) First-cycle voltage profiles with and without RMs at ~0.4 mA/cm^2. (b) Charging overpotentials. (c) Discharge capacities and (d) coulombic efficiencies for selected cells. (e,f) Nyquist plots before cycling and after six cycles.

2.1 | Electrochemistry of RMs

Moving straight to applicability of the RMs, overall, the redox reversibility of these RMs is much better in electrolytes without $LiNO_3$ than in those containing $LiNO_3$, while the latter ones of course are more relevant for Li–S battery application in general (Figure 2) [5]. In more detail, the addition of $LiNO_3$ decreased the redox activity of DmFc (Figure 2a) and AQ (Figure 2c), while it inhibited that of DmMn (Figure 2b) and NHQ (Figure 2d). The decreasing reversibility observed for DmFc is perhaps due to partial consumption of its reduced species ($DmFc_{red}$, with a Fe^{II+} center) as the anodic peak appears with a lower current density than the cathodic peak. Our hypothesis is that upon reduction, NO_3^- is partially irreversibly reduced to, e.g., NO_2^-, responsible for the cathodic current below ~1.7–1.8 V (Fig. S1) [43], which might have another redox couple at a higher potential than that of $DmFc_{ox}/DmFc_{red}$, and can oxidize $DmFc_{red}$ on the reverse/anodic scan. The same can be true for the AQ, while both DmMn and NHQ simply are unstable.

From the distinct cathodic and anodic peaks in the CVs of the electrolytes without $LiNO_3$ (a–d), the reduction potentials of the RMs (vs. Li^+/Li) were determined as DmFc, 2.85 V; DmMn, 2.41 V; AQ, 2.30 V; and NHQ, 2.00–2.10 V, which are put in context by schematically adding them to common Li–S battery cell discharge (Figure 2e) and charge (Figure 2f) profiles. The high redox potential of DmFc implies that its reduced form ($DmFc_{red}$) dominates during the entire discharge process, making it mostly inactive toward PSs. In contrast, DmMn and AQ have redox potentials aligned closely to the first discharge plateau (2.40–2.30 V), suggesting that their reduced and oxidized forms coexist and may facilitate elemental sulfur to long-chain PSs ($n = 6$–8) conversion according to the gamma rule (Figure 2g). At potentials below 2.30 V, these RMs are fully electrochemically reduced and thus likely inactive. NHQ exhibits similar redox speciation and activity to AQ but at the second plateau (2.10–2.00 V), thereby targeting short-chain PSs ($n \leq 4$) (Figure 2e–g).

Upon charging events, half-oxidized AQ and DmMn, as well as fully oxidized NHQ, are all able to facilitate oxidation of Li_2S/Li_2S_2 to higher-order PSs (Figure 2f,g). Finally, DmFc, fully oxidized at near the end of charge, may assist in converting all PSs back to elemental sulfur (Figure 2f,g), thus completing the redox cycle. These differences highlight the role of DmFc as an oxidizing RM during charge, while the other RMs are capable of both oxidizing and reducing roles under appropriate conditions.

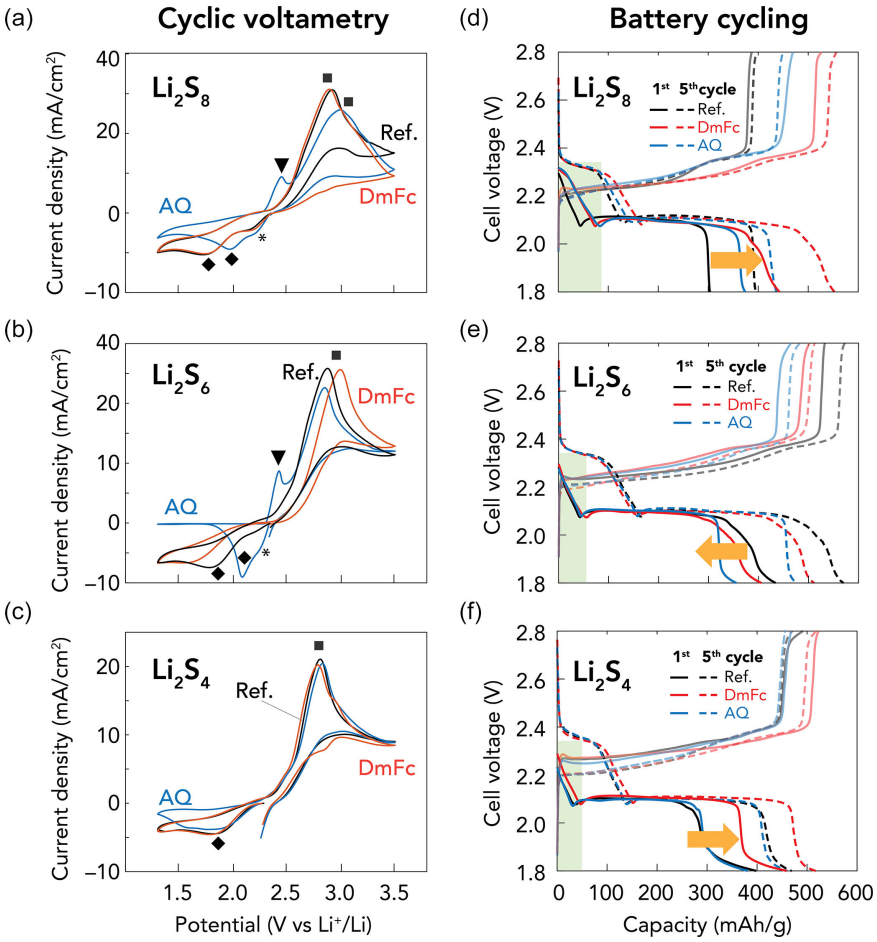

FIGURE 4 | (a–c) First-cycle cyclic voltammograms for Li–S battery cells based on Li_2S_8 (a), Li_2S_6 (b), and Li_2S_4 (c) catholytes, all recorded at 50 mV/s. The peak at 2.4 V (▼) is attributed to AQ oxidation, while other peaks originate from S/PS redox processes: 2.8 V (■, $S_{7,8}^{2-} \rightarrow S$), ~2.3 V (*, $S_{6,8}^{2-} \rightarrow S_4^{2-}$), and 2.0–2.1 V (♦, $S_4^{2-} \rightarrow S_2^{2-}/S^{2-}$). (d–f) Charge–discharge profiles of the first and fifth cycles of Li–S battery cells based on Li_2S_8 (d), Li_2S_6 (e), and Li_2S_4 (f) catholytes, all cycled at C/10 rate.

2.2 | Effect of RMs in Traditional Li–S Battery Cell Designs

The four RMs influenced the conventional Li–S battery cell in quite distinctly different ways. The reference cell, i.e. without any RM added to the electrolyte, displays the expected two-plateau discharge profile and can be fully charged for the first cycle without any noticeable PS shuttling—due to the presence of $LiNO_3$ [44, 45]. Introducing DmFc, DmMn, or AQ into the electrolyte led to a slight increase in the initial discharge capacity, whereas NHQ caused a capacity loss (Figure 3a). The DmMn-containing cell exhibited overcharging behavior (Figures 3a and S2) and subsequently failed to recharge. This behavior is attributed to the irreversibility of $DmMn_{red}/DmMn_{ox}$ under the presence of $LiNO_3$ (c.f. Figure 2b) and the high sensitivity of $DmMn_{red}$ ($[Cp^*_2Mn]^-$) to trace amounts of water and other electrophilic species [46, 47]. Thus, unlike the other RMs, DmMn does not function as a chemically stable and reversible RM, but rather promotes parasitic electrolyte decomposition and PS shuttling; it was therefore excluded from further investigation.

Clear differences in charging overpotential were observed between the RM-free and RM-containing cells as well as between the RM-containing cells (Figure 3b); AQ and DmMn lowered the overpotential by ~46 and 94 mV, respectively, whereas NHQ and DmFc yielded no noticeable changes. AQ, with its redox activity above the Li_2S oxidation potential region, effectively mediates the conversion of insulating discharge products and thereby reduces polarization [41]. The action of NHQ is explained by its resilience to reversed oxidation under the presence of $LiNO_3$, while DmFc remains inactive at voltages lower than its reduction potential (2.8 V).

Adding AQ also improved the capacity retention (Figure 3c,d); after 100 cycles at 0.1C, the AQ-containing cell retained 63% of its initial capacity and showed ~95% coulombic efficiency. The cell using DmFc showed no such improvement, which, again, is explained by its inactive role due to its very high reduction potential. The poor cyclability for the cells using NHQ (Figure 3c,d) and DmMn (Fig. S2) is in accordance with their instability toward $LiNO_3$.

With respect to the effect on charge transfer, the electrochemical impedance spectroscopy (EIS) data revealed some distinct differences in both interfacial resistance and capacitive behavior. Before cycling (Figure 3e), the cells with DmFc and DmMn showed increased interfacial resistance, but minimal impact using AQ and NHQ. Yet, a larger capacitance was observed for AQ, possibly due to π–π stacking on the carbon surface [48], but this was, however, not observed for NHQ. Moving to the data obtained after six cycles (Figure 3f), all the RM-containing cells exhibited a decreased charge transfer resistance as compared to the cell without any RM, confirming the role of RMs to facilitate interfacial redox reactions and promoting improved reaction kinetics.

2.3 | Effect of RMs in Catholyte-Based Li–S Battery Cells

Following the promising results for DmFc and AQ for traditional Li–S battery cells, we turned to examine their effect on Li_2S_8, Li_2S_6, and Li_2S_4 catholyte-based cells. As AQ is known to react with PSs [48], the RM-containing catholytes were expected to differ in PS speciation as well as RM redox states. This is indeed reflected in the first cycle CV data, where the cathodic peaks of the Li_2S_8 and Li_2S_6 catholytes shifted to higher potentials after adding AQ, while the shift for the Li_2S_4-based cell was negligible (Figure 4a–c). Notably, an oxidation feature of AQ at ~2.4 V was observed for the cells with Li_2S_8 and Li_2S_6 catholytes during the first cycle, but was absent in the Li_2S_4 catholyte-based cell. In the second cycle, however, this feature appeared in all cells, albeit at lower current density (Fig. S3), suggesting that AQ can be regenerated. In contrast, DmFc increased the overpotential only in the Li_2S_6 catholyte-based cell and had little influence on the other PSs (Figure 4a–c). Furthermore, the reduction and oxidation peaks of DmFc appeared only for the Li_2S_4 catholyte cell data, at 2.85 and 2.96 V, respectively.

These changes in PS speciation and redox states of RMs subsequently affected the cycling performance. For the Li_2S_8-based cells (Figure 4d), both RMs extended the ~2.3 V discharge plateau associated with long- to short-chain PS conversion, e.g., S_{6-8}^{2-} to S_{4-5}^{2-} [2], resulting in a capacity gain of ~20 mAh/g, and overall, the discharge capacities increased by ~80 mAh/g (AQ) and ~130 mAh/g (DmFc). In contrast, the Li_2S_6- and Li_2S_4-based cells (Figure 4e,f, respectively) showed no distinct high-voltage plateaus irrespective of any RM addition. Moreover, AQ and DmFc slightly suppressed the discharge capacity that is associated with the Li_2S deposition in the Li_2S_6-based cells, whereas the

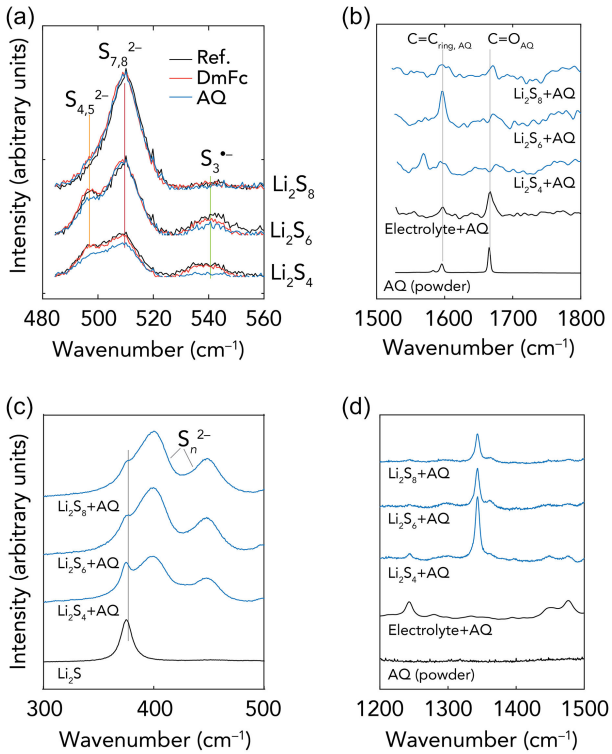

FIGURE 5 | (a) Raman spectra highlighting short- and long-chain PSs and $S_3^{\bullet-}$ radical in freshly prepared RM-free catholytes (Ref.) and RM-containing catholytes. (b) Spectral shifts of the bands of AQ [49] in AQ-containing PS catholytes. (c,d) Newly emerging spectral features in AQ-containing catholytes as compared to (c) Li_2S (powder) and (d) AQ dissolved in the electrolyte and AQ powder.

Li_2S_4-based cell was only improved by DmFc. This behavior of DmFc is consistent with what was observed above (c.f. Figure 3a) despite its inactive role at voltages below 2.8 V. We hypothesize that the activity of DmFc is triggered by partial chemical oxidation with, e.g., the reduction products of $LiNO_3$ that form upon contact with the lithium metal anode [5].

All cells could be charged to 2.8 V (Figure 4d–f) with a ~100–150 mAh/g overcharge, indicating effective reoxidation of Li_2S/Li_2S_2 to higher-order PSs and elemental sulfur, likely facilitated by $LiNO_3$. From the second to the fifth cycle (Figure S4 and Figure 4d–f, respectively), additional discharge features of ~100 mAh/g appear: a slope from 2.8 → 2.4 V and a plateau at 2.3 V, respectively, corresponding to sulfur-to-S_n^{2-} ($n = 6$–8) and long- to short-chain PS conversions. The consistent capacity trends relative to the first cycle suggest regeneration of RM during cycling, possibly mediated by preferential RM–PS interactions.

To identify the PS species which preferentially interact with DmFc and AQ, we employed Raman spectroscopy on freshly prepared catholytes (Figures 5 and S5). All RM-free catholytes display strong S–S stretching bands at 400 and 450 cm^{-1} corresponding to S_n^{2-} ($n = 4$–8) species (Fig. S5) [50, 51]. The relative proportion of long- and short-chain PSs is reflected by the intensity ratio between the ~510 cm^{-1} band ($S_{7,8}^{2-}$) [51, 52] and the ~490 cm^{-1} band (S_{4-6}^{2-}) [50, 53] (Figure 5b). In addition, the $S_3^{\bullet-}$ radical was detected at 534 cm^{-1} in RM-free Li_2S_6 and Li_2S_4 catholytes [50, 54, 55].

Upon addition of DmFc, the Raman spectra remain essentially unchanged across all catholytes (Figure 5a and S4), suggesting negligible interaction with any PSs, and this can be attributed to the predominance of nonreactivity of $DmFc_{red}$ toward PSs (c.f. Figure 2g). In stark contrast, AQ induces systematic changes in the Li_2S_6 and Li_2S_4 catholyte spectra, while the Li_2S_8 catholyte spectrum is largely unaffected. The changes include attenuation of the 490 cm^{-1} band of $S_{4,5}^{2-}$ and the 534 cm^{-1} band of $S_3^{\bullet-}$ (Figure 5a), alongside with spectral shifts in the bands of AQ (Figure 5b) and the concomitant growth of new features at 374 cm^{-1} and 1350 cm^{-1} (Figure 5c). These bands are assigned to the AQ-derived reduction product [48], with the former potentially overlapping—but distinct from Li_2S under this oxidative condition. Combined/separately, these reactions could modify the catholyte composition and thus account for different impacts of AQ on the performance of catholyte-based cells.

As these spectral changes are most prominent for the Li_2S_4 catholyte (Figure 5a–c), they suggest that AQ preferentially reacts with short-chain PSs and in addition may disturb some equilibria involving $S_3^{\bullet-}$ through more complicated pathways [56] than

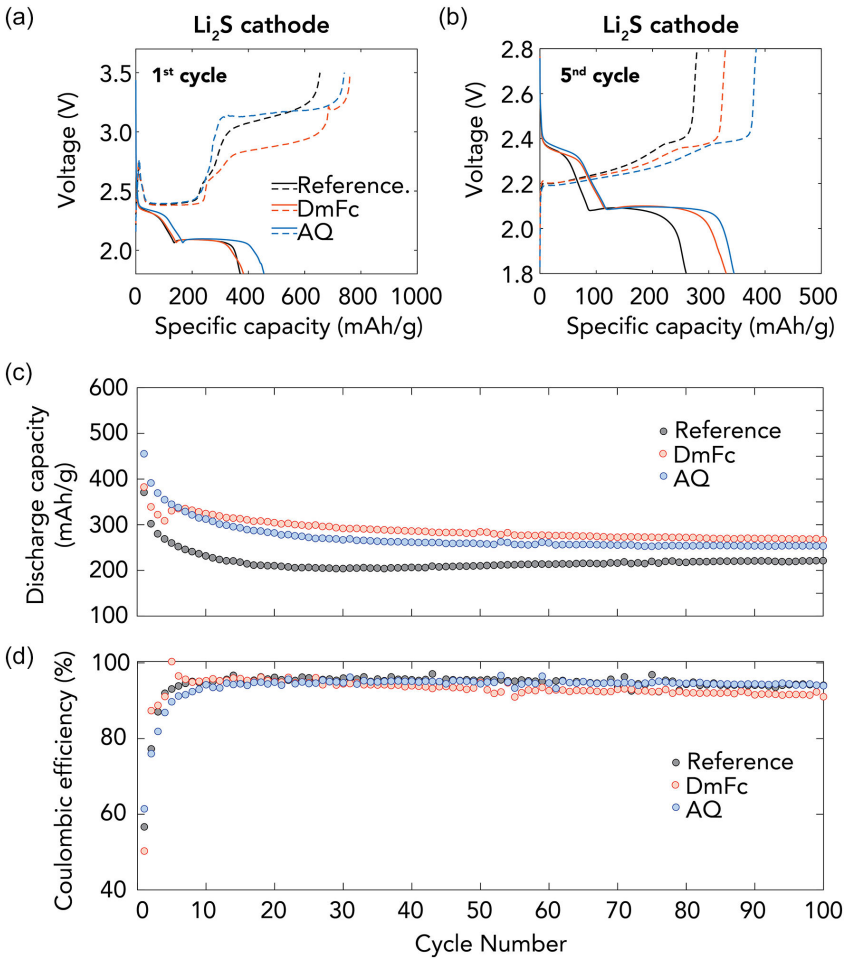

FIGURE 6 | Charge–discharge profiles of (a) the first cycle and (b) the fifth cycle of Li–S battery cells using Li_2S cathode. (c) Discharge capacities and (d) coulombic efficiencies of these cells.

the simple gamma rule. We note that these reactions would involve ~ 10% of the total PS concentration, assuming a 1:1 AQ:PS reaction stoichiometry (Table S1). However, they likely consume nearly all available AQ upon the mixing with Li_2S_4 catholyte (Figure 5b), thus neutralizing the mediator and resulting in the first cycle performance comparable to the RM-free cell. Furthermore, as AQ was only partially regenerated during the second cycle (Fig. S3), no significant improvement was observed (Fig. S4).

In contrast, these reactions consume less AQ in the Li_2S_8 and Li_2S_6 catholytes due to much lower concentration of short-chain PSs. The remaining AQ is thus available to facilitate the conversion of short-chain PSs produced gradually via electrochemically controlled processes, thereby enhancing sulfur utilization. This role may, however, still be compromised at the end of the second plateau when Li_2S starts depositing, as observed using the Li_2S_6 catholyte. We hypothesize that the effect on $S_3^{\bullet-}$ formation contributes to this effect by promoting film-like growth of Li_2S, which can passivate the electrode [57], rather than forming the distinct 3D crystalline structures which would otherwise enhance sulfur utilization [57, 58].

2.4 | Effect of RMs in Li_2S Cathode-Based Li–S Battery Cells

The effect of DmFc and AQ to enable a solution-phase and chemically assisted oxidation of Li_2S was then investigated by electrochemical cycling of Li_2S cathode-based cells (Figure 6). Due to the insulating nature of Li_2S and the resulting high activation barrier [23], all cells were initially charged up to 3.5 V [23, 24, 40] (Figure 6a). Here, DmFc decreased the overpotential of the second charge plateau, while AQ showed no difference vs. the reference cell, while during discharge, none of them affected the potential plateau, but AQ slightly enhanced the capacity. During the fifth cycles (Figure 6b), both AQ and DmFc reduced the overpotential during the second charge plateau and both increased the capacity.

From an application perspective, the above confirms that RMs not only reduce the initial charging overpotential but also enables a higher active material utilization, as seen by the higher capacities, including those of the stable long-term cycling, where the DmFc-containing cell showed slightly higher capacities during the first 100 cycles as compared to the AQ-containing one

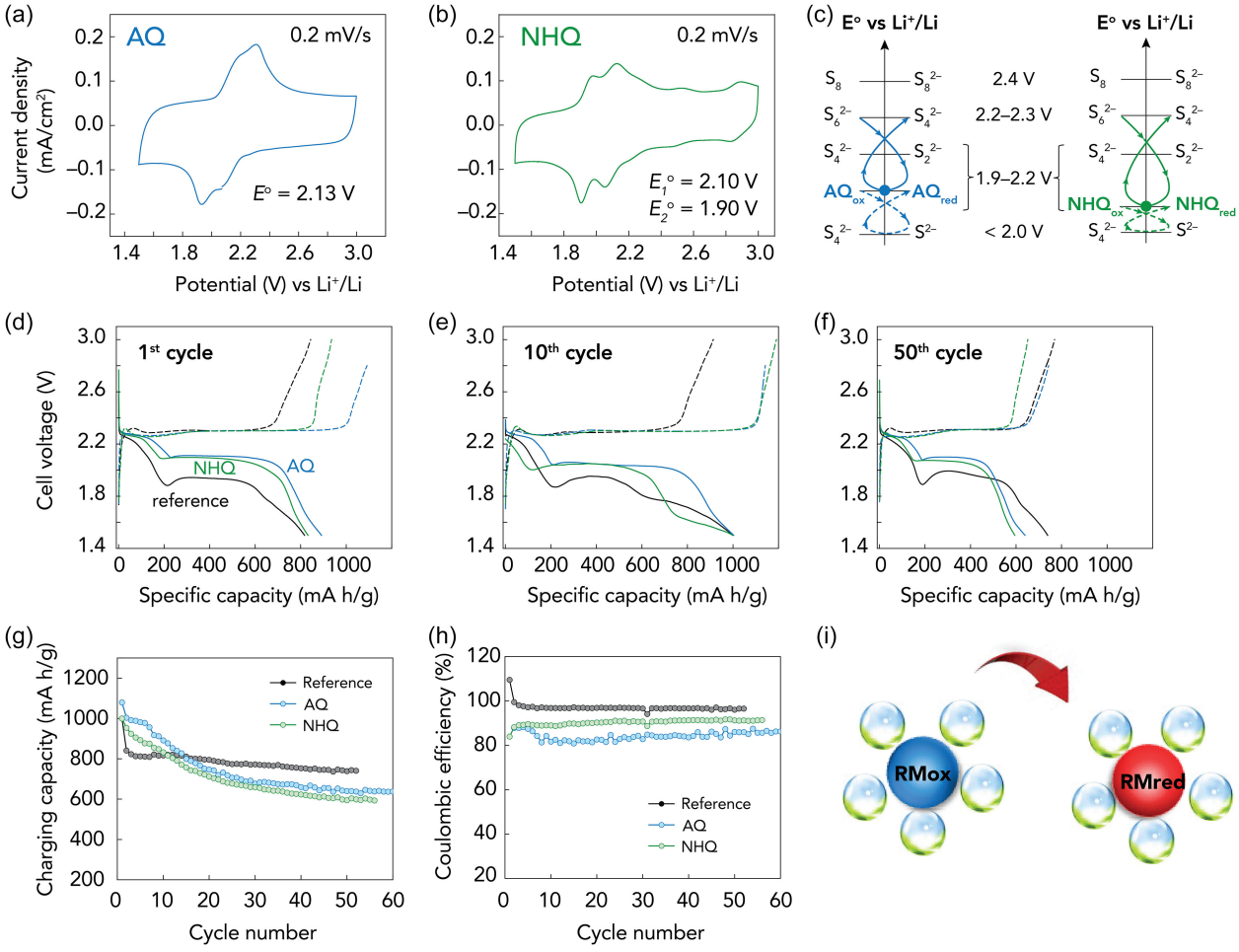

FIGURE 7 | Voltammograms of 1.0 M LiTFSI in TFEE:DOL electrolytes containing (a) AQ and (b) NHQ. (c) Schematic (not scaled) gamma rule of the AQ's and NHQ's reactivity toward PSs during charge (solid lines) and discharge (dash lines). Potential profiles of the first cycle (d), 10th cycle (e), and 50th cycle (f) of cells using the reference electrolyte (without RM) and the RM-containing WSEs. (g) Charging capacities and (h) coulombic efficiencies. (i) Schematic representation of the solvent reorganization during the redox reaction.

(Figure 6c), whereas the coulombic efficiency was close to 95% for all cells (Figure 6d). It should be noted that the coulombic efficiency is lower than that of S_8-based cathodes. This can be attributed to the Li_2S/C electrode formulation employed here, which utilizes a simple porous carbon host. Such a design provides limited PS confinement, thereby promoting PS dissolution and subsequent shuttling to the Li metal anode, ultimately resulting in the observed lower coulombic efficiency.

2.5 | Effect of RMs in WSE-Based Li–S Battery Cells

To elucidate the influence of solvation on the reactivity of the RMs, we replaced DME by TFEE to create a WSE. In WSEs based on fluorinated ether solvents such as TFEE, the solubility of long-chain PSs is low due to poor Li^+ solvation [59], leading to accumulation of PSs near the cathode [53], and thus, RMs were expected to play a more pronounced role when using a WSE. For the same reason, no $LiNO_3$ is required in the TFEE-based electrolyte, thereby avoiding possible problematic side reactions (c.f. Figure 2). Given the performance of AQ shown above for various Li–S battery designs, we choose to focus on AQ and furthermore we compare with NHQ, whose redox activity is not hindered in the absence of $LiNO_3$.

Using the WSE, both AQ and NHQ retained their redox reversibility at *ca.* 2.1 V, with AQ displaying a slightly higher current density (Figure 7a,b). As this is within the second discharge plateau of Li–S battery cells, this suggests, in stark contrast to the DME-based electrolytes, that both half-reduced AQ and NHQ provide comparable effects on the reduction of short-chain PSs ($n \leq 4$), and the fully oxidized species of both RMs facilitate oxidation of Li_2S to higher-order PSs during charge (Figure 7c).

This changed RM redox reactivity was also reflected in the Li–S battery cell performance (Figure 7d–h), foremost a longer first discharge plateau (by ~80 mAh/g) and a higher voltage for the second plateau (Figure 7d). The initial discharge capacities were comparable, but the charge capacity increased in the presence of RMs, with the stronger effect from AQ, which also decreased the overpotential significantly. The discharge capacities continuously slightly improved for 10 cycles (Figure 7e) but then declined (Figure 7f). In contrast, the charge capacity increased (Figure 7g), suggesting some overcharging phenomenon, likely attributable to enhanced PS shuttling and incomplete oxidation of short-chain PSs. Overall, the presence of RMs considerably lowered the coulombic efficiency (Figure 7h). This behavior can be attributed to enhanced mobility of short-chain polysulfides (PSs), likely induced by RM-mediated sulfur conversion. These shorter-chain species are more soluble and mobile [53], which promotes their diffusion toward the Li metal anode, thereby intensifying shuttle reactions and leading to reduced coulombic efficiency. Hence, neither AQ nor NHQ was as effective during charging as expected, likely due to solubility limitations of either the reduced and/or the oxidized forms of the RMs in the WSE. As solvent reorganization (Figure 7i) plays a crucial role during redox reactions and directly influences the reaction kinetics (i.e., Marcus theory [60, 61]), the lower solvating ability of fluorinated solvents, here TFEE, may hinder the reorganization step during the RM redox process, rendering the reaction irreversible or incomplete.

3 | Conclusions

Our comparative investigation of metallocene- and quinone-based RMs reveals that their effectiveness depends on sulfur speciation and electrolyte composition. AQ enhances the electrochemical performance across multiple Li–S battery concepts, whereas DmFc exhibits selective activity toward short-chain PSs (e.g., S_4^{2-}) and Li_2S, but has limited impact on elemental sulfur utilization. Electrochemical and spectroscopic results indicate that AQ preferentially reacts with short-chain PSs and/or $S_3^{\bullet-}$, which explains its reduced effectiveness in the short-chain PS-rich catholyte cell but enhanced sulfur utilization in systems where long-chain PS or sulfur dominates the redox chemistry. On the other hand, DmMn and NHQ consistently degrade the performance of the conventional cell, likely due to instability or parasitic reactions with the $LiNO_3$ contained in the electrolyte.

However, the expected benefits of quinone-based RMs are diminished when using a WSE, highlighting the importance of both RM and/or PS solubility and solvent reorganization kinetics. Collectively, our findings identify AQ as a comparatively robust and versatile RM for Li–S batteries, while also emphasizing that RM performance is inseparable from electrolyte composition and especially solvent solvation properties and charge transfer kinetics—why codesign of RMs and electrolytes is a must—and provide guidance for future rational design of RMs for Li–S batteries.

4 | Experimental Section

4.1 | Chemicals and Materials

Lithium bis(trifluoromethanesulfonyl)imide (LiTFSI, Solvionic, 99.99% <20 ppm H_2O) and $LiNO_3$ (Sigma–Aldrich, 99.99%) were dried at 140°C for 24 h under vacuum. 1,3-Dioxolane (DOL, Sigma–Aldrich, 99.8% 75 ppm BHT), 1,2-dimethoxyethane (DME, Sigma–Aldrich, 99.9%), and 1,2-(1,1,2,2-tetrafluoroethoxy)ethane (TFEE) were stored with pre-activated 3 Å molecular sieves (300°C under vacuum for 24 h). Prior to use, the dry solvents were filtered with a syringe filter. The water content was regularly checked by Karl–Fischer titration and was typically 3–5 ppm. Decamethyl ferrocene (DmFc, Sigma–Aldrich, 99.98%), decamethyl manganocene (DmMn, Sigma–Aldrich, 99.98%), anthraquinone (AQ, Acros Organics, 98%), 1,4-bis(methylamino)9,10-anthraquinone (NHQ, Alfa Aesar, 95%), Li_2S (Sigma–Aldrich, 99.98%), sulfur (Sigma–Aldrich, 99.98%), 1-methyl-2-pyrrolidon (NMP) (Sigma–Aldrich, analytical standard), and polyvinylidene fluoride (PVDF) (Alfa Aesar) were all used as received. C/S composite (60 wt% S ≈ 2.5 mg_S/cm^2) cathodes were provided by ISIT Fraunhofer within the Horizon 2020 project HELIS. Porous carbon cathodes were purchased from Vulcano. The Li_2S cathodes were prepared by mixing Li_2S powder with carbon black in a mortar, followed by the addition of PVDF as a binder dissolved in NMP solvent. The component ratio was Li_2S:carbon black:PVDF = 60:30:10 by weight. The resulting slurry was stirred overnight at room temperature and subsequently cast onto aluminum foil. The loading of the Li_2S cathodes was 2.16–3.57 mg_{Li2S}/cm^2. We used Whatman glass fiber (GF, 260 µm) and Celgard polymer membrane for separators. All chemicals and materials were stored in an Ar-filled glovebox (with O_2 and water levels below 1 ppm).

4.2 | Electrolyte and Catholyte Preparation

All electrolytes and catholytes were prepared inside the Ar-filled glovebox. The reference electrolyte, 1.0 M LiTFSI, with or without 0.3 M $LiNO_3$ in DME:DOL, was prepared by first mixing the two solvents—DME and DOL—at a 1:1 volume ratio, followed by the addition of appropriate amounts of LiTFSI and either $LiNO_3$ or not. The reference WSE, composed of 1.0 M LiTFSI in TFEE:DOL (1:1, v/v), was prepared similarly. RM-containing electrolytes were prepared by additionally dissolving the corresponding amount of DmFc, DmMn, AQ, or NHQ to achieve 20 mM.

The catholytes were prepared by first mixing S_8 and Li_2S powders to the corresponding Li:S stoichiometry and concentration of 0.19–0.22 mol/L of the final PS chain length (Li_2S_8, Li_2S_6, and Li_2S_4) according to Rauh et al. [62] (Table S1). After adding a fixed volume of the reference electrolyte [1.0 M LiTFSI + 0.3 M $LiNO_3$ in DME:DOL (1:1 v/v)], the mixtures were stirred at 60°C for 24 h. The 20 mM RM-containing catholytes were made by adding appropriate amounts of DmFc, DmMn, AQ, or NHQ.

4.3 | Electrochemical Testing

All electrochemical measurements were performed at 25°C using CR2032 coin cells assembled in the Ar-filled glovebox. To evaluate the electrochemical reversibility of RMs, cyclic voltammetry (CV) was performed on cells composed of (i) a ∅13 mm porous carbon-coated aluminum working electrode, (ii) a ∅15 mm lithium metal foil counter and reference electrode, and (iii) a ∅16 mm GF separator soaked with 80 µL of electrolyte. CVs were recorded using a Biologic VSP instrument with a scan rate of 0.2 mV/s over a voltage window of 1.5–3.2 V vs. Li^+/Li°. The formal reduction potential (E^o) of each RM was determined by averaging the anodic and cathodic potentials [63].

The coin cells used a lithium metal anode, and either a C/S composite, porous carbon, or Li_2S cathode (∅13 mm), and a Celgard separator soaked with 70 µL of electrolyte or 30 µL of catholyte. All cells were cycled between 1.8 and 2.8 V vs. Li^+/Li° at a C/10 rate using a Scribner 580 Battery Test System, where the theoretical capacities (C) used for elemental sulfur, Li_2S_8, Li_2S_6, and Li_2S_4 were 1672, 1390, 1301, and 1133 mAh g^{-1}, respectively. EIS was performed at the initial state before any cycling, and at the end of the sixth discharge–charge cycle. The applied DC voltage was 10 mV, the frequency swept from 1 MHz to 100 mHz, and a rest of 10 s was applied before each data acquisition.

4.4 | Raman Spectroscopy

Raman spectra were collected by using a coherent sapphire laser (488 nm, 33 mW) and a Nd:YAG laser (1064 nm, 400 mW) to complement the spectral regions that are affected by photoluminescence. All measurements were carried out at 25°C on ~100 µL of the freshly prepared electrolytes/catholytes which were initially loaded into 1 mm quartz cuvettes and subsequently sealed inside the Ar-filled glovebox. Spectra obtained with the 488 nm laser were performed on a LabRam HR Evolution (Horiba GmbH) spectrometer equipped with a Syncerity OE detector, a 200 µm confocal hole, and a 50× long-working distance objective focused into the liquid phase inside the quartz cuvette. Spectra acquisition was done with 60 accumulations of 60 s exposure, and an 1800 grooves/mm grating was used to achieve high-resolution spectra (~0.3 cm^{-1}) in the 100–700 cm^{-1} region (S–S vibration modes) and the 1200–1500 cm^{-1} region (AQ-derived products). Spectra with the 1064 nm excitation were carried out on a Bruker MultiRAM FT-Raman spectrometer equipped with a liquid nitrogen cooled Ge-diode detector. These spectra, with a resolution of 4 cm^{-1}, were acquired by averaging 1000 scans over the 50–2000 cm^{-1} range. Baseline correction and spectral normalization were performed in MATLAB (version R2025b, The MathWorks, Inc.).

Acknowledgments

This work was financially supported by the Swedish Research Council's (VR) Distinguished Professor grant "Next Generation Batteries" (#2021-00613) to P. J. and received funding through the European Union's Horizon 2020 research and innovation program under grant agreement no. 666221, "High-Energy Lithium-Sulfur Cells and Batteries" (HELIS). P. J. and S. S. R. especially acknowledge the 2-year EMJMD scholarship offered by the EU within the frame of the MESC+ program, an ERASMUS MUNDUS Master Course.

Funding

This research was funded by Swedish Research Council's (VR) (#2021-00613) and European Union's Horizon 2020 research and innovation (666221).

References

1. P. G. Bruce, S. A. Freunberger, L. J. Hardwick, and J.-M. Tarascon, "Li–O2 and Li–S Batteries with High Energy Storage," *Nature Materials* 11 (2012): 19–29.

2. M. Wild, L. O'Neill, T. Zhang, et al., "Lithium Sulfur Batteries, a Mechanistic Review," *Energy & Environmental Science* 8 (2015): 3477–3494.

3. Y. V. Mikhaylik and J. R. Akridge, "Polysulfide Shuttle Study in the Li/S Battery System," *Journal of the Electrochemical Society* 151 (2004): A1969.

4. X. Li, X. Pu, S. Han, et al., "Enhanced Performances of Li/Polysulfide Batteries with 3D Reduced Graphene Oxide/Carbon Nanotube Hybrid Aerogel as the Polysulfide Host," *Nano Energy* 30 (2016): 193–199.

5. S. Xiong, K. Xie, Y. Diao, and X. Hong, "Properties of Surface Film on Lithium Anode with LiNO3 as Lithium Salt in Electrolyte Solution for Lithium–sulfur Batteries," *Electrochimica Acta* 83 (2012): 78–86.

6. Q. Zou and Y.-C. Lu, "Solvent-Dictated Lithium Sulfur Redox Reactions: An Operando UV–vis Spectroscopic Study," *The Journal of Physical Chemistry Letters* 7 (2016): 1518–1525.

7. A. Gupta, A. Bhargav, and A. Manthiram, "Highly Solvating Electrolytes for Lithium–Sulfur Batteries," *Advanced Energy Materials* 9 (2019): 1803096.

8. X. Gao, Z. Yu, J. Wang, et al., "Electrolytes with Moderate Lithium Polysulfide Solubility for High-Performance Long-Calendar-Life Lithium–sulfur Batteries," *Proceedings of the National Academy of Sciences* 120 (2023): e2301260120.

9. Z. Shi, S. Thomas, D. Guo, et al., "Solvation Sheath Reorganization by Alkyl Chain Tuning Promises Lean-Electrolyte Li–S Batteries," *ACS Energy Letters* 9 (2024): 5391–5402.

10. A. Kottarathil, Z. Slim, H. A. Ishfaq, et al., "The Role of the Anion in Concentrated Electrolytes for Lithium-Sulfur Batteries," *Journal of the Electrochemical Society* 171 (2024): 070506.

11. E. S. Shin, K. Kim, S. H. Oh, and W. I. Cho, "Polysulfide Dissolution Control: the Common Ion Effect," *Chem. Commun* 49 (2013): 2004–2006.

12. T. Ishikawa, S. Haga, K. Shigenobu, et al., 2024. *Faraday Discussions*.

13. X. Yu and A. Manthiram, "A Class of Polysulfide Catholytes for Lithium–sulfur Batteries: Energy Density, Cyclability, and Voltage Enhancement," *Physical Chemistry Chemical Physics* 17 (2015): 2127–2136.

14. R. D. Rauh, K. M. Abraham, G. F. Pearson, J. K. Surprenant, and S. B. Brummer, "A Lithium/Dissolved Sulfur Battery with an Organic Electrolyte," *Journal of the Electrochemical Society* 126 (1979): 523.

15. G. Liu, Q. Sun, Q. Li, J. Zhang, and J. Ming, "Electrolyte Issues in Lithium–Sulfur Batteries: Development, Prospect, and Challenges," *Energy & Fuels* 35 (2021): 10405–10427.

16. H. Pan, X. Wei, W. A. Henderson, et al., "On the Way Toward Understanding Solution Chemistry of Lithium Polysulfides for High Energy Li–S Redox Flow Batteries," *Advanced Energy Materials* 5 (2015): 1500113.

17. S. S. Zhang and J. A. Read, "A New Direction for the Performance Improvement of Rechargeable Lithium/Sulfur Batteries," *Journal of Power Sources* 200 (2012): 77–82.

18. M. Agostini, D.-J. Lee, B. Scrosati, Y. K. Sun, and J. Hassoun, "Characteristics of Li2S8-Tetraglyme Catholyte in a Semi-Liquid Lithium–sulfur Battery," *Journal of Power Sources* 265 (2014): 14–19.

19. M. Agostini, S. Xiong, A. Matic, and J. Hassoun, "Polysulfide-Containing Glyme-Based Electrolytes for Lithium Sulfur Battery," *Chemistry of Materials : A Publication of the American Chemical Society* 27 (2015): 4604–4611.

20. G. Zhou, E. Paek, G. S. Hwang, and A. Manthiram, "Long-Life Li/Polysulphide Batteries with High Sulphur Loading Enabled by Lightweight Three-Dimensional Nitrogen/Sulphur-Codoped Graphene Sponge," *Nature Communications* 6 (2015): 7760.

21. R. Demir-Cakan, M. Morcrette, A. G. Gangulibabu, R. Dedryvère, and J.-M. Tarascon, "Li–S Batteries: Simple Approaches for Superior Performance," *Energy & Environmental Science* 6 (2012): 176–182.

22. Y. Son, J.-S. Lee, Y. Son, J.-H. Jang, and J. Cho, "Recent Advances in Lithium Sulfide Cathode Materials and Their Use in Lithium Sulfur Batteries," *Advanced Energy Materials* 5 (2015): 1500110.

23. H. Ye, M. Li, T. Liu, Y. Li, and J. Lu, "Activating Li_2S as the Lithium-Containing Cathode in Lithium–Sulfur Batteries," *ACS Energy Letters* 5 (2020): 2234–2245.

24. Y. Yang, G. Zheng, S. Misra, J. Nelson, M. F. Toney, and Y. Cui, "High-Capacity Micrometer-Sized Li_2S Particles as Cathode Materials for Advanced Rechargeable Lithium-Ion Batteries," *Journal of the American Chemical Society* 134 (2012): 15387–15394.

25. D. Liu, C. Zhang, G. Zhou, et al., "Catalytic effects in lithium–sulfur batteries: promoted sulfur transformation and reduced shuttle effect,"*Advancement of Science* 5 (2018): 1700270.

26. J. Zhou and A. Sun," Defect engineering enables an advanced separator modification for high-performance lithium-sulfur batteries",*Chemical Engineering Journal* 495 (2024): 153648.

27. H. Sies, R. J. Mailloux, and U. Jakob, "Fundamentals of Redox Regulation in Biology," *Nature Reviews Molecular Cell Biology* 25 (2024): 701–719.

28. A. Hagfeldt, U. B. Cappel, G. Boschloo, et al., In Solar Cells (Second Edition (2013). 385–441.

29. W.-J. Kwak, H. Kim, H.-G. Jung, D. Aurbach, and Y.-K. Sun, "Review—A Comparative Evaluation of Redox Mediators for Li-O_2 Batteries: A Critical Review," *Journal of the Electrochemical Society* 165 (2018): A2274.

30. H. Al Salem, G. Babu, C. V. Rao, and L. M. R. Arava, "Electrocatalytic Polysulfide Traps for Controlling Redox Shuttle Process of Li–S Batteries," *Journal of the American Chemical Society* 137 (2015): 11542–11545.

31. Y.-J. Li, J.-M. Fan, M.-S. Zheng, and Q.-F. Dong, "A Novel Synergistic Composite with Multi-Functional Effects for High-Performance Li–S Batteries," *Energy & Environmental Science* 9 (2016): 1998–2004.

32. Z.-L. Xu, S. J. Kim, D. Chang, et al., "Visualization of Regulated Nucleation and Growth of Lithium Sulfides for High Energy Lithium Sulfur Batteries," *Energy & Environmental Science* 12 (2019): 3144–3155.

33. C. Zheng, S. Niu, W. Lv, et al., "Propelling Polysulfides Transformation for High-Rate and Long-Life Lithium–sulfur Batteries," *Nano Energy* 33 (2017): 306–312.

34. G. Zhou, H. Tian, Y. Jin, et al., "Catalytic Oxidation of Li_2 S on the Surface of Metal Sulfides for Li–S Batteries," *Proceedings of the National Academy of Sciences* 114 (2017): 840–845.

35. Z. Yuan, H.-J. Peng, T.-Z. Hou, et al., "Powering Lithium–Sulfur Battery Performance by Propelling Polysulfide Redox at Sulfiphilic Hosts," *Nano Letters* 16 (2016): 519–527.

36. Z. Sun, J. Zhang, L. Yin, et al., "Conductive Porous Vanadium Nitride/Graphene Composite as Chemical Anchor of Polysulfides for Lithium-Sulfur Batteries," *Nature Communications* 8 (2017): 14627.

37. T.-G. Jeong, D. S. Choi, H. Song, et al., "Heterogeneous Catalysis for Lithium–Sulfur Batteries: Enhanced Rate Performance by Promoting Polysulfide Fragmentations," *ACS Energy Letters* 2 (2017): 327–333.

38. J. Liang, L. Yin, X. Tang, et al., "Kinetically Enhanced Electrochemical Redox of Polysulfides on Polymeric Carbon Nitrides for Improved Lithium–Sulfur Batteries," *ACS Applied Materials & Interfaces* 8 (2016): 25193–25201.

39. F. Y. Fan, W. C. Carter, and Y-Ming Chiang, "Mechanism and Kinetics of Li_2S Precipitation in Lithium–Sulfur Batteries," *Advanced Materials* 27 (2015): 5203–5209.

40. S. Meini, R. Elazari, A. Rosenman, A. Garsuch, and D. Aurbach, "The Use of Redox Mediators for Enhancing Utilization of Li_2S Cathodes for Advanced Li–S Battery Systems," *The Journal of Physical Chemistry Letters* 5 (2014): 915–918.

41. Y. Tsao, M. Lee, E. C. Miller, et al., "Designing a Quinone-Based Redox Mediator to Facilitate Li2S Oxidation in Li-S Batteries," *Joule* 3 (2019): 872–884.

42. R. S. Assary, L. A. Curtiss, and J. S. Moore, "Toward a Molecular Understanding of Energetics in Li–S Batteries Using Nonaqueous Electrolytes: A High-Level Quantum Chemical Study," *The Journal of Physical Chemistry C* 118 (2014): 11545–11558.

43. S. S. Zhang, "Effect of Discharge Cutoff Voltage on Reversibility of Lithium/Sulfur Batteries with $LiNO_3$ -Contained Electrolyte," *Journal of the Electrochemical Society* 159 (2012): A920.

44. D. Aurbach, E. Pollak, R. Elazari, G. Salitra, C. S. Kelley, and J. Affinito, "On the Surface Chemical Aspects of Very High Energy Density, Rechargeable Li–Sulfur Batteries," *Journal of the Electrochemical Society* 156 (2009): A694.

45. S. S. Zhang, "A New Finding on the Role of LiNO3 in Lithium-Sulfur Battery," *Journal of Power Sources* 322 (2016): 99–105.

46. M. Malischewski and K. Seppelt, "Structural Characterization of Potassium Salts of the Decamethylmanganocene Anion $Cp^*_2Mn^-$," *Dalton Transactions* 48 (2019): 17078–17082.

47. J. L. Robbins, *United States*, 1981.

48. G. Li, X. Wang, M. H. Seo, et al., "Chemisorption of Polysulfides through Redox Reactions with Organic Molecules for Lithium–sulfur Batteries," *Nature Communications* 9 (2018): 705.

49. K. K. Lehmann, J. Smolarek, O. S. Khalil, and L. Goodman, "Vibrational Assignments for the Raman and the Phosphorescence

Spectra of 9,10-Anthraquinone and 9,10-Anthraquinone-d8," *The Journal of Physical Chemistry* 83 (1979): 1200–1205.

50. J. Hannauer, J. Scheers, J. Fullenwarth, B. Fraisse, L. Stievano, and P. Johansson, "The Quest for Polysulfides in Lithium–Sulfur Battery Electrolytes: An Operando Confocal Raman Spectroscopy Study," *ChemPhysChem* 16 (2015): 2755–2759.

51. T. Chivers, F. Edelmann, J. F. Richardson, and K. J. Schmidt, "Convenient Synthesis, X-Ray Crystal Structure, and Raman Spectrum of the Heptasulphide Dianion, S_7^{2-}, in $[PPN]_2S_7 \cdot 2EtOH$," *Canadian Journal of Chemistry* 64 (1986): 1509–1513.

52. R. Steudel, F. Schuster, and Z. Naturforsch, "X-Ray Structural Analyses of Cyclodecasulfur (S10) and of a Cyclohexasulfur-Cyclodecasulfur Molecular Addition Compound (S6 • S10)[1]." *A: Physical Science* 32 (1977): 1313–1319.

53. R. Bouchal, A. Boulaoued, and P. Johansson, "Monitoring Polysulfide Solubility and Diffusion in Fluorinated Ether-Based Electrolytes by Operando Raman Spectroscopy," *Batteries & Supercaps* 3 (2020): 397–401.

54. T. Chivers and I. Drummond, "Characterization of the Trisulfur Radical Anion S3- in Blue Solutions of Alkali Polysulfides in Hexamethylphosphoramide," *Inorganic Chemistry* 11 (1972): 2525–2527.

55. R. J. H. Clark, T. J. Dines, and M. Kurmoo, "On the Nature of the Sulfur Chromophores in Ultramarine Blue, Green, Violet, and Pink and of the Selenium Chromophore in Ultramarine Selenium: Characterization of Radical Anions by Electronic and Resonance Raman Spectroscopy and the Determination of Their Excited-State Geometries," *Inorganic Chemistry* 22 (1983): 2766–2772.

56. Y.-C. Lu, Q. He, and H. A. Gasteiger, "Probing the Lithium–Sulfur Redox Reactions: A Rotating-Ring Disk Electrode Study," *The Journal of Physical Chemistry C* 118 (2014): 5733–5741.

57. H. Pan, J. Chen, R. Cao, et al., "Non-Encapsulation Approach for High-Performance Li–S Batteries through Controlled Nucleation and Growth," *Nature Energy* 2 (2017): 813–820.

58. H. Chu, H. Noh, Y.-J. Kim, et al., "Achieving Three-Dimensional Lithium Sulfide Growth in Lithium-Sulfur Batteries Using High-Donor-Number Anions," *Nature Communications* 10 (2019): 188.

59. S. Drvarič Talian, S. Jeschke, A. Vizintin, K. Pirnat, I. Arčon, G. Aquilanti, P. Johansson, and R. Dominko, "Fluorinated Ether Based Electrolyte for High-Energy Lithium–Sulfur Batteries: Li^+ Solvation Role Behind Reduced Polysulfide Solubility," *Chemistry of Materials* 29 (2017): 10037–10044.

60. R. A. Marcus, "On the Theory of Oxidation-Reduction Reactions Involving Electron Transfer. I," *The Journal of Chemical Physics* 24 (1956): 966–978.

61. R. A. Marcus and N. Sutin, "Electron Transfers in Chemistry and Biology," *Biochimica et Biophysica Acta (BBA)* 811 (1985): 265–322.

62. R. D. Rauh, F. S. Shuker, J. M. Marston, and S. B. Brummer, "Formation of Lithium Polysulfides in Aprotic Media," *Journal of Inorganic and Nuclear Chemistry* 39 (1977): 1761–1766.

63. N. Elgrishi, K. J. Rountree, B. D. McCarthy, E. S. Rountree, T. T. Eisenhart, and J. L. Dempsey, "A Practical Beginner's Guide to Cyclic Voltammetry," *Journal of Chemical Education* 95 (2018): 197–206.

Supporting Information

Additional supporting information can be found online in the Supporting Information section.